Atmos. Meas. Tech. Discuss., 8, 5283–5327, 2015
www.atmos-meas-tech-discuss.net/8/5283/2015/
doi:10.5194/amtd-8-5283-2015

Atmospheric Measurement Techniques Discussions
Open Access

Synergy of stereo cloud top height and ORAC optimal estimation cloud retrieval: evaluation and application to AATSR

D. Fisher[1,*], **C. A. Poulsen**[2], **G. E. Thomas**[2], **and J.-P. Muller**[1]

[1]Imaging Group, Mullard Space Science Laboratory, University College London, Holmbury St. Mary, Dorking, Surrey, RH5 6NT, England, UK
[2]Rutherford Appleton Laboratory, Didcot, Oxfordshire, UK
[*]now at: Earth and Environmental Dynamics Research Group, Department of Geography, King's College London, The Strand, WC2R 2LS, London, UK

Received: 25 March 2015 – Accepted: 4 May 2015 – Published: 27 May 2015

Correspondence to: D. Fisher (daniel.fisher@kcl.ac.uk)

Published by Copernicus Publications on behalf of the European Geosciences Union.

Abstract

In this paper we evaluate the retrievals of cloud top height when stereo derived heights are combined with the radiometric cloud top heights retrieved from the ORAC (Optimal Retrieval of Aerosol and Cloud) algorithm. This is performed in a mathematically rigorous way using the ORAC optimal estimation retrieval framework, which includes the facility to use independent a priori information. Key to the use of a priori information is a characterisation of their associated uncertainty.

This paper demonstrates the improvements that are possible using this approach and also considers their impact on the microphysical cloud parameters retrieved. The AATSR instrument has two views and three thermal channels so is well placed to demonstrate the synergy of the two techniques. The stereo retrieval is able to improve the accuracy of the retrieved cloud top height when compared to collocated CloudAerosol Lidar and Infrared Pathfinder Satellite Observations (CALIPSO), particularly in the presence of boundary layer inversions and high clouds. The impact on the microphysical properties of the cloud such as optical depth and effective radius was evaluated and found to be very small with the biggest differences occurring over bright land surfaces and for high clouds. Overall the cost of the retrievals increased indicating a poorer radiative fit of radiances to the cloud model, which currently uses a single layer cloud model. Best results and improved fit to the radiances may be obtained in the future if a multi-layer model is used.

1 Introduction

Clouds play a key role in the Earth's climate system and have long been recognised as important moderators of the atmosphere, strongly modulating both incoming shortwave (SW) and outgoing longwave (LW) radiation. At short wavelengths, due to the global fractional cloud occurrence being on the order of 0.6 to 0.7 (Stubenrauch et al., 2013), they lead to an approximate doubling of the Earth's average albedo from 0.15 to 0.3

AMTD
8, 5283–5327, 2015

(Cess, 1976) and impart a strong cooling effect. At long wavelengths, clouds absorb and re-emit outgoing LW radiation leading to a warming effect, especially at high altitudes. The magnitudes of the conflicting radiative components are in turn dependent on a number of microphysical (cloud optical depth, particle size) and macrophysical (fraction, altitude) cloud parameters. Observational analyses demonstrate that when the components are combined, the current overall radiative effect of clouds is one of SW cooling (Ramanathan et al., 1989; Ardanuy et al., 1991; Kiehl et al., 1994; Wielicki et al., 1996; Kiehl and Trenberth, 1997; Allen, 2011), but there is significant spatial heterogeneity. Due to the conflicting radiative effects and strong spatial variability, effective incorporation of cloud radiative behaviour into climate models is tremendously challenging and is one of the main causes of uncertainty in projecting the future state of the climate (Wetherald and Manabe, 1988; Cess et al., 1989, 1990, 1996; Colman, 2003; Soden and Held, 2006; Webb et al., 2006; Soden et al., 2008; Andrews et al., 2012; Zelinka et al., 2013; Sherwood et al., 2014). Reducing this uncertainty has been identified by the International Panel on Climate Change (IPCC, Stocker et al., 2013) as a key requirement for improving consensus between climate projections and therefore, gaining a better understanding of the future state of the climate. In order to reduce the uncertainties related to cloud more detailed and informative tests of the cloud parameterisation schemes employed in a climate models are required (Stephens, 2005). Such analysis can be achieved through assessing a model's ability to replicate cloudy conditions of the present day, which necessitates the use of observational data. In particular observational data that is accurate, consistent, long-term, well characterised, and global in scope.

Satellite-borne instruments well fulfil these requirements, and there are now numerous observational methods capable of retrieving both macro- and microphysical cloud properties. An excellent assessment of the most prominent algorithms and sensors is provided in Stubenrauch et al. (2013). Most retrieval algorithms tend to rely on absolute radiometric measurements, with cloud microphysical observations being derived from channels in the visible and near-infrared (Nakajima et al., 1990) and cloud macrophys-

AMTD
8, 5283–5327, 2015

ical observations being derived separately from infrared measurements using brightness temperatures, and algorithms such as the IR-split window method (Rossow and Garder, 1993) or CO_2 slicing (Menzel et al., 1983).

The ORAC (Optimal Retrieval of Aerosol and Cloud) algorithm (Poulsen et al., 2012; Watts et al., 1998) employs the optimal estimation approach (Rogers, 2000) based on radiometric retrieval principles and has been extensively applied to the Along Track Scanning Radiometer Instruments (ATSR), specifically ATSR-2 (1995–2008; Mutlow et al., 1999) and the Advanced-ATSR (2002–2012, Llewellyn-Jones et al., 2001, AATSR). The radiometric configuration of ATSR-2 and AATSR comprises seven channels at 0.55, 0.67, 0.87, 1.6, 3.7, 11 and 12 µm and enables the ORAC optimal estimation algorithm to effectively retrieve both macro- and microphysical cloud properties. Uniquely, in order to ensure LW and SW radiative consistency, the algorithm fits a physically consistent model of cloud to observations spanning shortwave and thermal channels, the visible to the infrared, extracting information on the height, optical depth, and particle size, whilst rigorously treating model and observation errors. This approach provides detailed estimation of the uncertainty in the retrieved quantities, and a quantification of the "goodness of fit" of the observations to the cloud forward model.

All radiometric approaches, irrespective of the algorithm employed, are known to suffer from poor performance in a number of common cloud conditions (Baum and Wielicki, 1994; Rossow et al., 2005; Garay et al., 2008; Menzel et al., 2008; Marchand et al., 2010). For example, Sayer et al. (2011) provides important caveats to the use of ORAC cloud optical depth retrievals in multi-layer cloud systems, and for cloud effective radius in the case of ice clouds. A pertinent assessment of the problematic cloud conditions for macrophysical retrievals using radiometric methods is presented in Marchand et al. (2010). In particular, boundary layer stratocumulus clouds, trade cumulus/broken clouds, high thin clouds such as cirrus, and multilayer cloud systems are identified as being very challenging for the radiometric approaches, with substantial biases in the retrieved CTH (Cloud Top Height). The Marchand et al. (2010) study demonstrates the potential for the application of the geometric approach afforded by stereo capable

AMTD
8, 5283–5327, 2015

instruments – in this instance the Multi-angle Imaging SpectroRadiometer (Moroney et al., 2002; Muller et al., 2002, 2006, 2013) – for the effective determination of macrophysical cloud parameters in cloud conditions which are challenging for radiometric approaches.

The ATSR instrument makes use of a dual-view conical scanning set up, with an initial observation in the forward direction along the satellite track at a 55° viewing zenith angle (decreasing to 47° viewing zenith angle at the edges of the forward scan) and a second observation at nadir with a viewing zenith angle of 2° (increasing to 22° viewing zenith angle at the edges of the nadir scan). The ATSR series of instruments has a long time series, IR channels from 1991 and visible/IR channels until 2012, and will be followed on by SLSTR (Sea and land surface Temperature Radiometer) in the near future. The instrument's detectors are low noise and well calibrated with on board visible and IR calibration systems, making it ideal to study cloud trends. The arrangement of the ATSR instrument facilitates the application of stereo-photogrammetric techniques for the determination of macrophysical cloud properties. In turn, this allows for the synergistic application of both geometric and radiometric macrophysical cloud parameter retrieval from a single instrument. Many groups are now using optimal estimation techniques to estimate cloud properties (e.g. Heidinger et al., 2010; Watts et al., 1998), however the capability of OE to include a priori information is not always utilised due to a lack of collocated information of sufficient accuracy and independence. Heidinger et al. (2010) have used climatological data as a priori information with mixed results, OCA (Optimal Cloud Analysis) and ORAC use European Centre for Medium-range Weather Forecasting (ECMWF) ERA Interim reanalysis sea surface temperature data as a priori to the surface temperature state vector. High resolution Spinning Enhanced Visible and InfraRed Imager (SEVIRI) visible imagery can be used to provide a priori cloud fraction. A priori cloud top height data is difficult to identify because of the high temporal variability of the cloud parameters. This work reports on the first instance of independent, collocated CTH data being used to achieve more accurate CTH retrievals. This synergistic application of a geometric and radiometric approach is evaluated in

AMTD
8, 5283–5327, 2015

terms of macro- and microphysical impacts, using the AATSR instrument in combination with the ORAC retrieval and the census stereo algorithm (Zabih and Woodfill, 1994).

The next section introduces the ORAC cloud retrieval algorithm. This is followed in Sect. 3 by a description of the stereo algorithm. In Sect. 4 the method for the synergistic application of the radiometric and geometric approaches, in this instance the application of the stereo derived CTH as an a priori into the ORAC retrieval, is given. The effect of the inclusion of a priori data on the performance of the ORAC retrieval in terms of cloud macrophysics is then considered through an inter-comparison against lidar derived cloud top layer (CTL) elevations from the Cloud-Aerosol Lidar with Orthogonal Polarization (CALIOP) instrument. For cloud microphysics a self-comparison between the ORAC retrieval with and without a priori data is undertaken. In Sect. 6 a discussion of the outcomes of Sect. 5 is presented. Finally conclusions are drawn in Sect. 7.

2 Optimal estimation cloud retrieval algorithm

The ORAC algorithm (Poulsen et al., 2012; Watts et al., 1998) is an optimal estimation retrieval that can be used to determine both aerosol and cloud properties from visible/infrared satellite radiometers. In the case of cloud retrievals the algorithm fits radiances computed from LUTs created from DIScrete Ordinates Radiative Transfer (DISORT) (Stamnes et al., 1988) to the TOA (Top of Atmosphere) signal measured by the satellite by varying the cloud optical depth, effective radius cloud top pressure, phase and surface temperature simultaneously. The result of retrieving all parameters by varying all channels simultaneously is a radiatively consistent set of cloud properties. The cloud retrieval has thus far been applied to ATSR-2 and AATSR, as well as SEVIRI, Advanced Very High Resolution Radiometer (AVHRR) and MODerate Resolution Imaging Spectroradiometer (MODIS) in the context of the ESA Climate Change Initiative (CCI) programme (Stengel et al., 2013).

AMTD
8, 5283–5327, 2015

The optimal estimation (OE) framework of ORAC provides several key advantages:

- The ability to include prior knowledge of the retrieved quantities is inbuilt into the method. In previous OE cloud retrievals the only constraint has been on the retrieval of surface temperature and is provided by the ERA Interim reanalysis.
- The retrieval provides comprehensive uncertainty propagation, allowing measurement uncertainty, forward model uncertainty (due to approximations and assumptions which must be made in the modelling to TOA radiance) and uncertainties in a priori knowledge to be combined to give a rigorous estimate of the uncertainty on retrieved values on a pixel by pixel basis.
- SW/LW radiative effects of cloud can be readily computed from the fitted cloud model and is ensured to be consistent with the observed radiances.

Algorithm Description:

- ORAC uses "on the fly" radiative transfer; the method relies on fitting the measurements, to within expected error limits, to the predicted values. Since exact methods are far too slow, the strategy adopted then is to utilise "fast", non-exact, radiative transfer models with analytical gradients. This is achieved by decoupling the cloud and "cloud free atmosphere" parts of the system. The former component is stored in precalculated multiple scattering cloud radiative properties look-up tables (LUTs), while clear atmosphere radiance and transmission calculations are performed on-line using the RTTOV radiative transfer code for both the visible and infrared channels.
- ORAC requires knowledge of the surface reflectance for each visible/near-infrared channel, which is provided by MODIS surface BRDF products (MCD43B) over land and a sea surface reflectance model over the ocean (Sayer et al., 2010). The surface temperature is a retrieved parameter, with the emissivity at each thermal channel determined using the University of Wisconsin-Madison Baseline Fit Emissivity Database (Seemann et al., 2008).

AMTD
8, 5283–5327, 2015

– The cloud and clear-atmosphere radiative properties and surface properties are merged into a three-layer (below cloud, cloud and above cloud) system by relatively straightforward and computationally efficient equations.

– ORAC uses MIE scattering for water droplets and optical properties from Baran et al. (2005) for ice crystals.

– The ORAC algorithm currently assumes a single cloud layer and retrieves cloud optical depth, cloud top pressure, cloud effective radius, cloud fraction and sea surface temperature, associated uncertainty and goodness fit metric. From these retrieved products liquid and ice water paths can then be calculated.

ORAC code is an open source community code currently being applied to AATSR, AVHRR and MODIS to create long-term climate records of cloud properties, and is available for download from http://proj.badc.rl.ac.uk/orac.

3 Stereo-photogrammetric cloud top height determination

3.1 Stereo technique

The stereo-photogrammetric approach relies on the principle of parallax: the distance (or height) dependent displacement of a stationary object when observed from two or more different viewing angles or positions. The only ancillary data requirement is an accurate knowledge of the geometry of the instrument, which enables stereo reconstruction, the conversion of the displacements in the imagery (disparities) into real world observations. In comparison to radiometric cloud retrievals a number of distinct advantages can be defined:

– Stereo retrievals are dependent on the geometry of the imaging system, not the radiometric fidelity. Therefore, they are calibration independent.

AMTD
8, 5283–5327, 2015

– Multi-layer cloud systems do not introduce biases to the stereo retrieved CTHs. The stereo retrieval will return the altitude of the feature with the greatest contrast.

– Stereo retrievals require very little ancillary data to retrieve CTH. In the case of ATSR, knowledge of the geometry of the instrument is the sole requirement. This significantly reduces the number of sources of uncertainty in the product.

The ATSR instruments stereo-photogrammetric capabilities have been exploited variously (Lorenz, 1985; Shin and Pollard, 1999; Prata and Turner, 1997; Muller et al., 2007; Seiz, 2003; Fisher et al., 2014). In terms of application to CTH retrieval, the most recent study is that by Muller et al. (2007) and involved the development of the M4 stereo image matching algorithm, which was influenced by the development of similar stereo algorithms applied to the MISR instrument (Muller et al., 2002). Here, based on work undertaken by Hirschmuller and Scharstein (2009), we apply the non-parametric census stereo algorithm (Zabih and Woodfill, 1994) to derive CTH. This approach has been demonstrated to be the most effective area based stereo matcher for imagery with simulated radiometric distortions similar to those found in EO derived data. As such, the census algorithm is applied in all cases in this study and is described in the following section.

3.2 Non-parametric stereo matching algorithm

The basic premise of the census stereo matching algorithm is to replace each image pixel with a descriptive bit vector that encodes the pixel pattern of the pixel's local neighbourhood. A bit is set in the vector if the corresponding pixel in the local neighbourhood is of a lesser intensity than the pixel of interest. The use of bits effectively limits the influence of statistically outlying pixels on the pixel of interest during correction for radiometric dissimilarity. It is also unaffected by all radiometric distortions as long as they do not alter the pixel ordering. For any pixel x we can define the census transformation as,

$$\Gamma(x) = \otimes f(x, n) \quad (1)$$

AMTD
8, 5283–5327, 2015

Where $\otimes$ is a concatenation operator which concatenates the results of the comparison function, f, to the bit vector, Γ. The comparison function takes as arguments x, the pixel of interest on which a window N is centred, and n, a pixel from the set that comprises the comparison window, i.e. $n \in N$. The comparison function evaluates to 1 if $n < x$ and 0 if $n \geq x$. The bit vector and the comparison window have the same size. Here, N is set to a radius of 7 pixels (Γ of length 49) as this provides suitable discriminative power for effective stereo matching whilst not increasing computational cost significantly.

Applying Eq. (1) to every pixel in both the reference and comparison images yields two 3-D arrays of bits vectors. In order to locate the correspondences the Hamming distance metric is used to compare the bit vectors as follows,

$$S\left(x_{i,j}, u_r, v_r\right) = \sum \Gamma^R_{i,j} \vee \Gamma^C_{i+u_{r,j}+v_r} \tag{2}$$

where the cost S for a given pixel x at the reference image location i, j is determined for r different across and along track displacements, u and v. This is achieved by summing the *exclusive or* comparisons, as determined by the *exclusive or* operator $\vee$, between the reference bit vector, Γ^R, at location i, j and comparison image bit vector, Γ^C, at the displaced location $i + u_r, j + v_r$. The costs for all disparity assessments are aggregated by a 7 pixel radius mean filter to reduce noise. Following cost aggregation a simple spline interpolation routine is employed to estimate sub-pixel disparities in the along-track direction from the along-track disparities associated with the five smallest costs. Across track disparities are returned at integer level accuracy.

3.3 Post-processing

The disparities returned by the census algorithm are defined within the imaging coordinate system, and as such, are not physically representative of the measure of CTH. To convert from disparity to CTH a camera model, which replicates the ATSR imaging geometry, is employed to assign each disparity estimate to an above ellipsoid elevation

AMTD
8, 5283–5327, 2015

estimate (Denis et al., 2007). Prior to conversion to elevations, the disparities are first corrected using the AATSR co-registration correction coefficients as defined in (Fisher and Muller, 2013). The accuracy of the elevation estimates from the Census transform varies by channel. For the 11 micron channel, employed in all cases in this study, inter-comparison studies against elevations from the GMTED2010 DEM (Danielson and Gesch, 2011) and CTH observations from CALIOP (Winker et al., 2009) return RMSE statistics of approximately 500 and 1200 m respectively.

In order to differentiate between the surface and CTH observations the GMTED2010 DEM is used. Any pixel with an elevation that is more than 500 m above the collocated surface elevation is flagged as a cloud feature with an associated CTH.

A further check is performed on a cloudy pixel to determine if it is located over a surface covered in snow and/or ice, as the census algorithm (and most other stereo matching algorithms) tends to be confused by the textureless/homogenous nature typical of such surface types, leading to erroneous CTH retrievals. Each orbit is therefore screened for snow/ice pixels using the clear snow/ice mask developed by Istomina et al. (2010) and any flagged pixel is set to a null value. The last step in the post processing is to set all edge pixels to a null value, to remove stereo processor edge artifacts.

4 Stereo as a priori

In the current implementation of ORAC for the CCI programme the first guess and a priori CTHs are set using the temperature of the 10.8 µm channel and an ECMWF temperature profile. As the 10.8 µm channel and ECMWF temperature profile are used by ORAC itself in determining CTH, this cannot be considered a prior constraint; thus the a priori is given essentially infinite (10^8) uncertainty, which results in a flat probability function and no prior constraint. In this configuration, the value determined from the temperature is essentially providing a first guess value only.

AMTD
8, 5283–5327, 2015

The setting of the a priori uncertainty is important: too tight and the retrieval will converge to the a priori and ignore the information in the measurements; too loose and the value of the prior information is lost. One example of the use of prior constraint in CTH retrievals is the use of CALIPSO climatological data in the AVHRR Pathfinder Atmospheres – Extended (PATMOS-X) product (Heidinger et al., 2010). Using climatological a priori (not collocated in time or space) maybe a technically sound approach to achieve more accurate height retrievals, particularly in the case of thin cirrus, however this is not appropriate when constructing a new, longer-term climatology. In this case the retrievals will converge toward the climatological values reducing the independence and hence reliability of the resulting time series, particularly in detecting long-term changes in CTH.

The optimal estimation algorithmic framework encourages the incorporation of independent a priori information, such as stereo derived CTH, but it is critical that the a priori data employed be truly independent information. Here, the assumption made is that despite being derived from the same instrument, the fundamental algorithmic differences between the radiometric ORAC and geometric census stereo approaches impart observational independence on the derived CTHs.

The assumption is justified because:

- The stereo retrievals are insignificantly affected by systematic noise e.g. those introduced by calibration errors.
- The random error contained within a central pixel, and the average random error of the local neighbourhood of that central pixel will be uncorrelated. Therefore the random errors in the ORAC retrieval, which is pixel based, and the stereo retrieval, which is area based, will also be uncorrelated. Furthermore, ATSR has specifically been designed to have very low noise in the IR channels in order to retrieve sea surface temperature at high accuracy (i.e. less than 20 mK, Smith et al., 2012).

AMTD
8, 5283–5327, 2015

– The error in the stereo matching is dominated by temporal changes between the views and geometric effects, neither of which correlate directly with the measurement error.

The a priori uncertainties for the stereo CTH data are determined through an inter-comparison against the CALIOP lidar using the dataset employed in Sect. 5 using the following method:

– The AATSR stereo CTH are quantised into 1 km bins.

– For each bin the constituent AATSR CTHs are differenced from their collocated CALIOP CTL elevations.

– The uncertainty at each bin is defined as the SD of these height differences.

– During the ORAC processing, each a priori CTH is assigned the uncertainty (SD) from its nearest height bin.

– Finally, as ORAC uses CTP values as a priori, the stereo CTH and CTH uncertainty are converted in CTP using geopotential height look up tables from the ECMWF ERA Interim reanalyses (Simmons et al., 2007).

The following section aims to assess where the incorporation of the census stereo CTH observations enhances the performance of ORAC and where they lead to degradation.

5 Inter-comparison of ORAC+Stereo with CALIOP observations

Two differing assessment are made in this section to evaluate the effect of including stereo a priori data in the ORAC retrieval: one focusing on the changes in the retrieved macrophysical characteristics; the other on the retrieved cloud microphysics. The only macrophysical parameter assessed is the CTH, as the other macrophysical parameter provided by ORAC – cloud fraction – is not impacted. The stereo data is not used as

AMTD
8, 5283–5327, 2015

a cloud mask; it only provides a priori CTH estimates and hence, it has no impact on the cloud flagging process in ORAC. The microphysical parameters assessed are cloud optical depth (COD) and cloud effective radius (RE).

The assessments for CTH and the microphysical parameters are undertaken using different comparison datasets. The CTH is assessed against CALIOP, using a dataset derived from AATSR and CALIOP collocations for the geographical region subset (latitudinal range: 50–85° N; longitudinal range: 80° W–5° E) explained in greater detail in Sect. 5.1. The limited, high latitude range of this dataset is necessary to obtain collocations within suitably defined time limits. The retrievals are evaluated separately over ice covered and ice free surfaces. As well as the limitations of the census algorithm over ice or snow surfaces, the ORAC retrievals are also expected to perform worse due to the difficulty in defining an accurate albedo and the increased difficulty of distinguishing clear-sky and cloud. In the analysis, it is assumed that all land areas are covered in ice (due to Greenland being the only substantial landmass in the geographical subset) and the AMSR-E sea-ice dataset (Spreen et al., 2008) is used to enable differentiation between ice covered and ice free (effectively open water) water bodies.

The changes in microphysical parameters are evaluated by inter-comparing the ORAC dataset with and without the stereo a priori, as the ORAC retrieval has already been extensively validated elsewhere (Sayer et al., 2011). From hereafter, ORAC when run employing census stereo a priori is referred to as ORAC+Stereo.

5.1 Comparison dataset and method

The CALIOP has been making measurements of clouds and aerosols since 2006. The instrument is carried on-board the CALIPSO satellite, which is located in the NASA A-Train satellite constellation and therefore has an equatorial overpass time of approximately 1:30 p.m. and a 16 day orbital repeat cycle. The on board CALIOP lidar has a ground footprint on the ellipsoid of 100 m and pulses every 333m along track. It receives backscattered radiation in three channels, two at 532 nm with sensitivity to the backscattered intensity at orthogonal polarisations and one at 1064 nm. The vertical

AMTD
8, 5283–5327, 2015

resolution is between 30–60 m depending on the altitude of the cloud, with 30 m resolution achievable in the troposphere (Vaughan et al., 2009). If the uppermost cloud layer has an optical depth of less than three (Vaughan et al., 2009), then CALIOP is able to detect the presence of lower cloud layers.

The AATSR data used in this comparison is the v2.0 RAL processed data product with calibration corrections provided by D. Smith at RAL (personal communication). There is an updated V2.1 processing available at RAL; however these data at present have not been evaluated for co-registration accuracy between the forward and nadir view, which is critical for accurate stereo CTH retrievals. The co-registration correction coefficients (Fisher et al., 2013) that are applied here were derived using v2.0 RAL processed, and are known to improve the co-registration accuracy to pixel level or better.

For the period April to October 2008, all collocated AATSR-CALIPSO orbits within the study region were extracted for this analysis, giving a total of 70 collocated orbits split between the months of April, July, August, September and October (no collocations fulfilling the requirements were found for May or June) with typically around 40 min between overpasses. The CALIOP L1 data is processed into various L2 products, of which the 1 km cloud product, CAL_LID_L2_01kmCLay-ValStage1-V3-01, is employed here for CTH analysis due to its similar resolution to the AATSR instrument. The lower limit for cloud detection for this product is a backscattered signal of greater than $1 \times 10^{-3}\,\mathrm{km}^{-1}\,\mathrm{sr}^{-1}$ (equivalent to an optical depth of 0.01 for cirrus clouds; McGill et al., 2007; Kahn et al., 2008; Vaughan et al., 2009).

The approach to generate the inter-comparison dataset generally follows that presented in Fisher et al. (2014) and proceeds as follows:

- A temporally collocated set of CALIOP 1 km L2 data, ORAC, ORAC+Stereo, and stereo a priori products are ingested.
- For each CALIOP 1 km sample, the associated latitude and longitude data are compared against the AATSR geographic grids.

AMTD
8, 5283–5327, 2015

– The geographically collocated AATSR pixel to that of the sample is determined by minimising the geographic distance using the Haversine formula. To be included in the analysis carried out here, the distance between the CALIOP sample and the closest AATSR pixel must be less than 5 km.

– Once collocated, all a priori stereo heights within a 5-by-5 pixel bounding box, centred on the geographically collocated AATSR pixel are considered. All of the a priori pixels within the bounding box are required to contain stereo derived estimates. This requirement is in place to ensure that the effect of including stereo as a priori is not lost in the analyses in the following sections (a priori estimates are not available for all ORAC+Stereo pixels, and in such instances ORAC and ORAC+Stereo use the same a priori values).

– Assuming all pixels within the bounding box contain a priori stereo CTH estimates the absolute distance between the CALIOP first cloud top layer (CTL) and the ORAC/ORAC+Stereo retrieved CTH is then computed. The pixel index within the bounding box which minimises the absolute distance is used to extract the following ORAC/ORAC+Stereo data: CTH; effective radius (RE); optical depth (COD); phase. The following data from the CALIOP sample is also recorded: CTL; cloud base layer (CBL); cloud phase; and number of cloud layers.

This collocation process has been carried out for all CALIOP samples with AATSR pixels within a 5 km radius across the entire temporally collocated dataset of 70 orbits.

5.2 Analysis of cloud top height

5.2.1 Retrieval comparison overview

The box-and-whisker plots presented in Fig. 1 provide a statistical overview of the CTH differences between the uppermost CALIOP CTL and the collocated ORAC, ORAC+Stereo and census stereo CTH retrievals derived using the approach described

AMTD
8, 5283–5327, 2015

in the last section. The order of operation employed is subtraction of the CALIOP CTL from the AATSR CTH for each assessment. In the analysis 10 different cloud feature combinations are assessed with a further differentiation based on the underlying surface type (land/not land), giving a total of 20 assessments. The 10 cloud feature combinations are as follows: very-high (CTL > 9 km) single-layer ice cloud; very-high (CTL > 9 km) multi-layer ice cloud; high (6 km < CTL ≤ 9 km) single-layer ice cloud; high (6 km < CTL ≤ 9 km) multi-layer ice cloud; mid (3 km < CTL ≤ 6 km) single-layer ice cloud; mid (3 km < CTL ≤ 6 km) multi-layer ice cloud; mid (3 km < CTL ≤ 6.5 km) single-layer water cloud; mid (3 km < CTL ≤ 6.5 km) multi-layer water cloud; low (CTL ≤ 3 km) single-layer water cloud; low (CTL ≤ 3 km) multi-layer water cloud. The feature classification of each collocated CALIOP/AATSR pixel is achieved using the CALIOP phase, number of layers, and the elevation of the uppermost CTL.

For very-high single-layer ice clouds the ORAC algorithm is shown in this analysis to be, on average, biased low to CALIOP by −1.85 and −2.43 km for very-high clouds over ice and non-ice surfaces respectively. When the stereo data is employed as a priori the low biases in the presence of very-high single-layer ice cloud in comparison to CALIOP are reduced, with an average low bias of −0.99 and −1.65 km for ice and non-ice surfaces. For very-high multi-layer ice clouds (where the uppermost CALIOP layer is ice) ORAC shows more substantial deviation from the uppermost CALIOP CTL, with mean low biases of < −3.2 km irrespective of surface type. When the stereo data is incorporated into the retrieval the magnitudes of the biases are again reduced, and do not exceed 2.35 km. The native stereo outputs are more consistent, and are almost unaffected by the number of cloud layers, with low biases typically around −1.2 km, indicating that the stereo technique, when applied to the AATSR 11 micron channels, is generally sensitive to the uppermost cloud layer, which has been demonstrated previously (Naud et al., 2007).

For high-level, single-layer and multi-layer ice clouds, the performance across all three approaches shows similar characteristics to the very-high cloud assessment at a reduced magnitude. For high, single-layer ice clouds the ORAC algorithm is shown

AMTD
8, 5283–5327, 2015

in this analysis to be, on average, biased low to CALIOP by −1.45 and −0.96 km for clouds over ice and non-ice surfaces respectively. When the stereo data is employed as a priori the low biases in the presence of high single-layer ice cloud in comparison to CALIOP are reduced, with an average low bias of −0.86 and −0.42 km for ice and non-ice surfaces. For high multi-layer ice clouds (where the uppermost CALIOP layer is ice) ORAC again shows more substantial deviation from the uppermost CALIOP CTL, with mean low biases of < −1.8 km irrespective of surface type. When the stereo data is incorporated into the retrieval the magnitudes of the biases are again reduced, and do not exceed 1.5 km. The native stereo outputs are more consistent, and are unaffected by the number of cloud layers, with low biases typically around −1 km.

For mid-level, single-layer ice clouds the performance across all three approaches is very similar with biases of < 1 km irrespective of surface type. For mid-level, multi-layer ice clouds (uppermost CALIOP layer is ice), ORAC and ORAC+Stereo show very similar behaviour over both surface types, with a slight decline in performance compared with single-layer cloud conditions as indicated by the increased range between the first and third quartiles. The stereo outputs again show similar performance irrespective of the number of cloud layers and surface type.

For mid-level, single-layer water clouds the performance across all three approaches is again very similar with biases of < 0.5 km irrespective of surface type. ORAC and ORAC+Stereo exhibit a slight decline in performance in mid-level multi-layer water cloud (uppermost CALIOP layer is water) situations with low biases approaching 1 km and substantially increased range between the first and third quartiles. The stereo heights present with similar behaviour for single and multi-layer water clouds and over each surface type. However, the stereo observations are noisier than the ORAC and ORAC+Stereo outputs, with ranges of ∼ 3 km between the first and third quartile values vs. < 200 m for ORAC and ORAC+Stereo for single-layer water clouds. The noise levels between the three different approaches are similar for multi-layer water clouds.

For low-level, single-layer water clouds ORAC and ORAC+Stereo share similar characteristics over water and ice covered surfaces with high biases of < 500 m vs. the

AMTD
8, 5283–5327, 2015

CALIOP CTL. The stereo outputs exhibit larger high biases approaching 1 km vs. the CALIOP CTL. The greater bias in the stereo outputs appears to be due to increased noise in the stereo matcher outputs for low level clouds as indicated by the large number of outliers. The outliers in the stereo dataset are likely caused by the smoothing effect of area-based stereo matching algorithms leading to incorrect disparity assignment at the interfaces between features at differing altitudes. In this instance, the disparities of higher cloud features are bleeding in to surrounding low cloud features. The performance for low-level, multi-layer water clouds (uppermost CALIOP layer is water) is similar for all three datasets.

5.2.2 Single-layer cloud

From the box-and-whiskers statistical CTH overview plots shown in Fig. 1 and the histogram analyses presented in Fig. 2 it is apparent that high ice clouds deserve closer inspection to better understand the impact of employing stereo data as an a priori. Another aspect, which is not clear from the box-and-whiskers plots (in part due to the CTH quantisation employed), but becomes apparent when looking at the profile plot shown in Fig. 3 and the histograms presented in Fig. 2 is the effect of incorporating stereo a priori data on the accuracy of CTH retrievals within the atmospheric boundary layer.

The error-bar plot shown in Fig. 4 presents the median height difference between CALIOP and the ORAC, ORAC+Stereo and stereo CTH outputs across sets of 500 m intervals for all single-layer clouds, with CTL altitudes determined by CALIOP to be between 6 and 12 km. The analysis here, however, focuses only on those multi-layer clouds with CTL altitudes as detected by CALIOP to be between 6 and 10.5 km, as at altitudes above 10.5 km, ORAC, ORAC+Stereo and census stereo all show similar low biased behaviour, with median height differences of around −1.5 km. For all three retrievals, the heights can be seen to be biased low vs. the CALIOP CTL for each height interval. The stereo retrievals are the least biased, and taking the average of the median differences for the height intervals between 6 and 10.5 km inclusive returns -0.4 ± 0.3 km. The ORAC retrieval without the stereo a priori is the most biased vs.

AMTD
8, 5283–5327, 2015

CALIOP returning -1.6 ± 1.2 km when the median height differences are averaged. When the stereo data are used as a priori there is a reduction in bias, although it still exceeds that of the stereo data, with an average median difference of -0.8 ± 0.5 km. As the cloud altitude increases there is a decrease in the low bias of the ORAC and ORAC+Stereo retrievals. Performing a linear regression on the median differences for the height intervals between 6 and 10.5 km returns slopes of −0.05 for stereo, −0.13 for ORAC+Stereo, and −0.34 for ORAC (excluding the 10.5 km median height difference for ORAC gives a slope of −0.2).

The error-bar plot shown in Fig. 5 presents the median height difference between CALIOP and the ORAC, ORAC+Stereo and stereo CTH outputs across sets of 500 m height intervals for all single-layer clouds between 0 and 3 km. For all clouds detected by CALIOP above 500 m altitude, there is good agreement between the datasets, with median height differences close to 0 km. However, for CTH retrievals with CALIOP observations with CTL altitudes in the 0–500 m range, the median differences for ORAC and the ORAC+Stereo show substantial divergence. The ORAC median difference is 1.32 km, the ORAC+Stereo, 0.29 km, and census stereo, 0.45 km. This indicates that the ORAC height assignments for clouds with altitudes of < 500 m are more often assigned with a high bias than when the stereo data is used as a priori. This result is also apparent in the screened histogram analyses in Fig. 2 with the ORAC plot showing substantially higher bin counts than ORAC+Stereo and stereo in the 2–4 km CTH range for CALIOP CTLs in the 0–2 km range. The explanation here is that the ORAC cloud top height is often assigned too high particularly where there is a boundary layer inversion and more than one temperature/height solution is possible. The stereo CTH provides an additional useful constraint that results in a correct height retrieval more often.

Generalising over all heights, cloud types and surface types we can say that, while the ORAC+Stereo bias it still larger than the stereo bias, the correlation has increased and the SD has decreased significantly indicating that the “noise” on the stereo retrieval is greatly reduced and the fine scale structure of the cloud top retained.

AMTD
8, 5283–5327, 2015

5.2.3 Multi-layer cloud

The error-bar plot in shown in Fig. 6 presents the median height difference between CALIOP and the ORAC, ORAC+Stereo and stereo CTH outputs across sets of 500 m intervals for all multi-layer clouds with the uppermost CTL altitudes determined by CALIOP to be between 6 and 12 km. The analysis here, however, focuses only on those multi-layer clouds with CTL altitudes as detected by CALIOP to be between 6 and 10.5 km. As with the single-layer high cloud analysis, at altitudes above 10.5 km ORAC, ORAC+Stereo and census stereo all show median height differences of typically < -2 km. The retrievals are again biased low vs. CALIOP, with similar behaviour in the case of single-layer clouds and with ORAC exhibiting the most low bias and stereo the least. The average median difference for ORAC is larger than with single-layer clouds at -2.4 ± 0.9 km as is the ORAC+Stereo at -1.3 ± 0.4 km. The stereo retrieval performs similarly to the single-layer cloud assessment, with an average median height difference of -0.4 ± 0.4 km. As the cloud altitude increases, in general, there is a decrease in the low bias of ORAC and the other retrievals perform with similar behaviour. Performing a linear regression on the median differences for the height intervals between 6 and 10.5 returns slopes of 0.05 for stereo, −0.06 for ORAC+Stereo, and −0.27 for ORAC.

5.3 Cloud optical property and retrieval cost analyses

Traditional cloud retrievals tend to perform height and microphysical property retrievals separately; however the problem with this technique is that it can be difficult to balance the LW and SW radiative effects of the clouds (Ham et al., 2009). While the visible and near infrared channels are mostly sensitive to the effective radius and optical depth, the Infra-red channels provide the most information about cloud top height with all channels contributing to a lesser or greater degree to all cloud properties. Hence it is important to evaluate the effect of modifying the cloud top height and its effect of the microphysical parameters.

AMTD
8, 5283–5327, 2015

The box-and-whiskers plots presented in Fig. 7 provide a statistical overview of the comparisons between ORAC and ORAC+Stereo, for cloud optical depth (COD) and effective radius (RE) split by whether the COD is greater or less than 10 (as determined by the ORAC retrieval). The box-and-whiskers plot presented in Fig. 8 provide a statistical overview of the costs for the ORAC algorithm with and without the stereo a priori. As with the CTH assessment in the previous section, the analysis looks at 10 different cloud feature combinations with a further differentiation based on the underlying surface type (land/not land), giving a total of 20 assessments. The 10 cloud feature combinations are the same as for the CTH assessment and the feature classification of each collocated CALIOP/AATSR pixel is also achieved using the CALIOP phase, number of layers, and the CTL data. The order of operation employed in this section is the subtraction of the ORAC+Stereo microphysical parameters from the ORAC microphysical parameters for each assessment.

As expected, the impact of the stereo cloud top height a priori on the microphysical retrievals is typically small with medians differences of close to zero across most analyses and features. For cloud optical depth, there are a number of cases where there are significant differences. This is particularly the case for ice clouds over icy surfaces when the cloud optical depth is > 10, where the combined mean difference is 25.7 ($\pm$13.1) optical depths vs. 12.1 ($\pm$3.0) optical depths for all other cases (excluding < 3 km multi-layer water cloud over ice). The largest COD difference is found for low-level multi-layer water clouds with optical depths of greater than 10, with a mean difference of 49. This result reflects in part the difficulty in retrieving cloud optical depth over bright surfaces as very small changes in reflectance can result in large COD changes and the difficulty in separating clouds from the surface. For less bright clouds with cloud optical depths of less than 10 the disagreement between ORAC and ORAC+Stereo is typically less than two to three.

For RE the behaviour for all cloud and surface types is similar and small compared with the typical retrieved values, the mean differences never exceeding $\pm 3\,\mu$m and median differences of approximately zero in all instances. Single layer ice cloud

AMTD
8, 5283–5327, 2015

with altitudes between 3–6 km present with a far larger range between the upper and lower quartiles of approximately 10, vs. < 5 for all other surface/cloud type combinations. While still small, these changes may reflect the impact of changes in the cloud phase from ice to water or vice versa induced by the a priori information within ORAC. Large changes in RE also occur for the clouds with smaller optical depth reflecting the stronger sensitivity of RE to the surface. Note that there is a degree of anti-correlation between COD and RE.

Typically the largest differences in optical depth and effective radius occur when the cloud is high, possibly mixed phase and/or multi layered. In these cases when the cloud top height is forced to a higher value by the prior constraint, the cloud top temperature is modified accordingly. This can cause a modification in the phase, effective radius and cloud optical depth, in order to reproduce the observed TOA brightness temperatures. This, in turn, will impact on the quality of fit achieved for the shortwave channels, and produce an increase in the retrieval cost function. This effect is clearly visible in Fig. 8, particularly for high ice clouds, where there are significant increases in high cost retrievals. In such cases the single-layer cloud assumption of the ORAC forward model simply is not an appropriate description of the real atmosphere.

The cost of the retrieval is an indicator of the goodness of fit between the forward modelled radiances/brightness temperatures and the satellite measurements. Provided the uncertainties have been estimated correctly, the cost has an expectation value equal to the number of measurements used (in this case 6). A high cost will generally be returned in ORAC in the presence of multi-layered cloud, or other scenario that does not fit the assumptions used in the retrieval. In nearly all cases, the costs increased when the stereo information was used. For low clouds the change in cost is small to negligible indicating that in the case of low clouds the stereo information still provides a good fit to the radiances and in the cases where the height has changed significantly, the retrieval has probably converged on the more accurate of the multiple solutions possible. For the higher cloud, the cost has increased significantly. This indicates that the ORAC+Stereo retrieved heights are no longer fitting as close to the single layer

AMTD
8, 5283–5327, 2015

cloud model as previously. This is to be expected and indicates more clearly that in many of these cases the cloud is multi layered.

The fact that the use of the stereo prior results in large increases in the retrieval cost for many multi-layer cloud observations suggests that it could form the basis of a method for detecting multi-layer cloud. This could prove very valuable, as a multi-layer cloud forward model is currently being implemented for ORAC, and determining when to apply it is a significant difficulty in its application.

6 Discussion

6.1 Impact on cloud top height retrieval

The analyses in Sect. 5 demonstrates that, for a number of different cloud conditions, the inclusion of stereo a priori data provides improvements in the ORAC CTH retrieval when compared to CALIOP. In the case of low clouds, such as stratocumulus, it is well known that radiative based retrieval algorithms, such as ORAC, typically exhibit CTH/CTP (Cloud Top Pressure) retrievals which are biased too low or too high depending on whether the temperature profile is searched for a temperature match to the TOA brightness temperatures from the surface up, or the top of the profiles down, respectively. In the case of ORAC the temperature profile is searched from the top down and consequently the cloud top height is often assigned too high. These biases are caused by the fact that low-level stratocumulus clouds often occur in the presence of temperature inversions, and the atmospheric temperature profiles employed to convert between the retrieved temperature and CTP often do not effectively represent either the strength or the position of the inversion. A clear example of this is in the CALIOP profile plot in Fig. 3, where the water cloud feature detected by CALIOP at approximately 500 m between the latitudes of 68 and 69° latitude is poorly captured by the ORAC retrieval, which instead assigns CTHs at around 2.5 km (likely the top of the temperature inversion). The census stereo approach relies on the geometry of the instrument

AMTD
8, 5283–5327, 2015

to assign height and therefore is completely independent of any temperature profile assumptions. In the case of boundary layer clouds, this leads to a significant reduction in bias in the retrieved CTHs as shown in the analysis in Sect. 5, and the profile plot in Fig. 3. The drawback of the stereo approach, aside from the fact that it only provides CTH, is a tendency to smooth the disparity field losing fine detail information on CTH. This effect is apparent in: the profile plot in Fig. 3 where the stereo heights entirely miss the fine scale detail of the cloud profile as determined by CALIOP; the census stereo output in the stereo CTH retrieval shown in Fig. 9, where the stereo algorithm misses much of the fine scale detail captured by ORAC. The effect is also apparent in the histogram in Fig. 2, particularly for CALIOP CTLs at altitudes between 2 and 6 km, where there is a small but significant under-estimation of the CTH by the census stereo algorithm, which is caused by the inability of the stereo algorithm to capture the finer scale CTH changes. Another potential drawback of the census stereo algorithm when applied to AATSR thermal channel is that it has a tendency to be noisy for low, particularly boundary layer, clouds, as demonstrated by the very large SDs (up to 4 km) in Fig. 5. This is also caused by the smoothing effect of the stereo algorithm. The drawbacks of the stereo algorithm, however, are somewhat mitigated (and the benefits retained), when employed as a priori in the ORAC retrieval. When combined, the accuracy of the ORAC+Stereo retrieval is better for the height assignment of low-level boundary layer clouds than census stereo applied to the thermal channel due to increased sensitivity to fine detail cloud structure, and substantially better than ORAC due to the improved a priori estimates providing the necessary constraint to overcome the inversion layer degeneracy.

Cirrus and other high altitude type cloud formations, if they have low optical depth, present a challenging cloud form to assign CTH to for both radiometric and geometric type algorithms. In the presence of a low optical depth cloud, the cloud top temperature retrieved by radiative based algorithms such as ORAC corresponds to a cloud top height typically 1 optical depth into the cloud, which for some clouds may not correspond with the true CTH but rather exhibit a significant low bias, particularly for optically

AMTD
8, 5283–5327, 2015

thin clouds with large vertical extent. For geometric type algorithms, the retrieved CTH is associated with the location within the cloud where the optical depth is sufficient to provide suitable image texture for reliable stereo image matching; this may be some way below the true cloud top. Note that the stereo algorithm uses the dual view capability of ATSR while the ORAC retrieval uses only the nadir view. Since the forward view has twice the path length though a cloud, the penetration depth is approximately half of the nadir view. This is consistent with the results presented in the histograms in Fig. 2, which demonstrate for clouds above 8 km that the census stereo observations tend to have reduced low biases (approx. half) than ORAC when compared to the CTL altitude as determined by CALIOP. This observation is made more concrete in Fig. 4 and the statistical analyses provided in Sect. 5.2, where the census stereo CTH retrievals, at least for clouds less than 11 km in altitude, typically have a much reduced low bias than the ORAC retrievals. It is likely that for clouds above 11 km in the inter-comparison regions that the optical depth is too low for any of the algorithms to perform effectively. When the stereo retrievals are incorporated into the ORAC retrieval as a priori the low bias is still present, but reduced. Further reductions in the ORAC+Stereo bias could potentially be achieved by reducing the uncertainties on the stereo a priori inputs for high clouds and by using the dual view in the ORAC cloud retrieval, both of which will be examined in the future.

Similar findings to those of single-layer high ice clouds are presented for the case of multi-layer clouds where the uppermost layer is above 6 km (and therefore ice). This is to be expected, as in the instances of optically thin cloud, rather than having the surface contributing to the observed radiance, it is instead the underlying cloud feature. However, the low biases in the ORAC retrievals for multi-layer clouds, as shown in Fig. 6, are generally larger than for the single-layer cloud case. This is likely due to the assumptions of the single layer cloud model employed by ORAC and the fact that in case of multi-layer clouds, the retrieved cloud top height is related to the effective radiance of the two layers, which will be an intermediate height. As with single-layer clouds when the stereo retrievals are incorporated into the ORAC retrieval as a priori

AMTD
8, 5283–5327, 2015

the low biases compared to the CALIOP CTL are generally reduced, but not to the same extent as stereo alone, due to the fact that the most radiometrically consistent cloud-top height remains below the height of the upper layer cloud layer if a single cloud layer is assumed. The stereo retrieval performs similarly irrespective of the number of cloud layers, and this is a feature of the geometric approach.

6.2 Impact on cloud optical properties and retrieval cost

One of the key benefits of combining the stereo in the OE retrieval is that in addition to cloud top height you can also retrieve consistent cloud properties such as optical depth and effective radius. The optical cloud properties analysis demonstrate that in general the optical properties are similar whether ORAC employs stereo a priori data or not. The largest differences in the retrievals have been shown to occur generally over regions of snow and ice, cloud with multi-layer or inhomogeneous vertical extent, and high optically thin clouds.

Such shortwave/long wave radiative inconsistency is common in cloud retrievals that perform separate micro and macrophysical. The future implementation of a multi layers cloud model will maintain the radiative consistency that can be invaluable for climate analysis.

7 Conclusions

For the first time, a synergistic application of radiometric and geometric cloud retrieval approaches has been carried out. This synergy was achieved using the AATSR instrument by employing census stereo derived CTHs as a priori inputs into the ORAC retrieval. The stereo derived a priori data act as constraints on the ORAC retrieval, constraining the range of the potential solutions of the optimal estimation algorithm. This technique makes optimal use of the design of the ATSR instrument: the stereo retrieval uses the ATSR-dual view to achieve accurate cloud top height assignment,

AMTD
8, 5283–5327, 2015

while ORAC uses well calibrated radiometric information to retrieve fine scale height information, cloud optical depth and effective radius. The techniques are combined using the optimal estimation framework which provides a mathematically rigorous way of accounting for the uncertainty on the a priori information.

The effect of the inclusion of the stereo a priori data has been evaluated for both cloud macro- and micro-physical properties. In terms of macrophysics an extensive inter-comparison was made against collocated CALIOP lidar observations for various cloud and surface types. The analyses result in a number of interesting findings. The inclusion of stereo derived a priori leads to a substantial improvement of the retrieval in the presence of boundary layer clouds reducing the median height difference vs. CALIOP for clouds at altitudes of less than 500 m from 1.32 km to 0.29 km, indicating a substantial reduction in high bias. This is particularly important as changes in boundary layer clouds, particularly marine boundary layer clouds, represent a particularly poorly constrained response to climate change in climate (Zelinka et al., 2013; Sherwood et al., 2014).

In the case of high single- and multi-layer clouds a reduction in low bias is found, with the average median difference for ORAC being −1.6 and then −0.8 km with the inclusion of stereo a priori, in the case of single layer clouds, −2.4 and then −1.3 km for multi-layer clouds. However, the stereo retrieved CTH from the 11 micron channel show far reduced low biases, with average median height differences of 0.4 km irrespective of cloud type. A future way to exploit the stereo information further would be to include the stereo information as a priori information in a multi-layer model, such a model is currently being developed by various groups (Watts et al., 2011). In terms of cloud microphysics, the inclusion of the stereo a priori usually has a limited impact on the retrieved parameters. Most differences appear to relate to the cloud type and bright surfaces, in particular high or multi-layer ice clouds for COD, and RE for all ice clouds.

The technique has the potential to be applied to the entire time series of ATSR data from 1990 to 2012 and to be applied to the follow on instrument SLSTR (Sea and Land surface Temperature instrument) which will be launched in 2015.

AMTD
8, 5283–5327, 2015

To summarise, the inclusion of stereo a priori data into the ORAC retrieval appears to improve performance in the presence of challenging cloud situations, particularly for boundary layer clouds and high-level ice clouds. The technique also highlights the consequences on the fit to the single layer model and the effects on the microphysical retrievals such as optical depth and effective radius and the consequences related to balancing the long wave and short wave radiative effective in a joint visible/IR single layer retrieval. More of the information in the stereo retrieval could be taken advantage of consistently when used in conjunction with a multi-layer model. It is worth noting that the technique demonstrated here is not limited to the ATSR series of instruments and cloud retrievals, but could be applied to ATSR retrievals of aerosol and aerosol layer height, particularly for desert dust storms, fire plumes and volcanic ash clouds, and also other multi view instruments such as MISR. The technique also has potential to be applied to multiple geostationary satellite instruments with overlapping fields of view.

Acknowledgements. Many thanks to Phil Watts for discussions on stereo data independence. This work has been funded by NCEO and by NERC under PhD studentship number NER/S/C/2006/14369 and uses the ESA CCI cloud algorithm code.

References

Andrews, T., Gregory, J. M., Webb, M. J., and Taylor, K. E.: Forcing, feedbacks and climate sensitivity in CMIP5 coupled atmosphere–ocean climate models, Geophys. Res. Lett., 39, L09712, doi:10.1029/2012GL051607, 2012.

Ardanuy, P. E., Stowe, L. L., Gruber, A., and Weiss, M.: Shortwave, longwave, and net cloud-radiative forcing as determined from Nimbus 7 observations, J. Geophys. Res.-Atmos., 96, 18537–18549, 1991.

Baum, B. A. and Wielicki, B. A.: Cirrus cloud retrieval using infrared sounding data – multilevel cloud errors, J. Appl. Meteorol., 33, 107–117, 1994.

Baran, A. J., Shcherbakov, V. N., Baker, B. A., Gayet, J. F., and Lawson, R. P.: On the scattering phase function of nonsymmetric ice crystals, Q. J. Roy. Meteor. Soc., 131, 2609–2616, 2005.

AMTD
8, 5283–5327, 2015

Cess, R. D.: Climate change: An appraisal of atmospheric feedback mechanisms employing zonal climatology, J. Atmos. Sci., 33, 1831–1843, 1976.

Cess, R. D., Potter, G. L., Blanchet, J. P., Boer, G. J., Ghan, S. J., Kiehl, J. T., Le Treut, H., Li, Z.-X., Liang, X.-Z., Mitchell, J. F. B., Morcrette, J.-J., Randall, D. A., Riches, M. R., Roeckner, E., Schlese, U., Slingo, A., Taylor, K. E., Washington, W. M., Wetherald, R. T., and Yagai, I.: Interpretation of cloud-climate feedback as produced by 14 atmospheric general circulation models, Science, 245, 513–516, doi:10.1126/science.245.4917.513, 1989.

Cess, R. D., Potter, G. L., Blanchet, J. P., Boer, G. J., Del Genio, A. D., Déqué, M., Dymnikov, V., Galin, V., Gates, W. L., Ghan, S. J., Kiehl, J. T., Lacis, A. A., Le Treut, H., Li, Z.-X., Liang, X.-Z., McAvaney, B. J., Meleshko, V. P., Mitchell, J. F. B., Morcrette, J.-J., Randall, D. A., Rikus, L., Roeckner, E., Royer, J. F., Schlese, U., Sheinin, D. A., Slingo, A., Sokolov, A. P., Taylor, K. E., Washington, W. M., Wetherald, R. T., Yagai, I., and Zhang, M.-H.: Intercomparison and interpretation of climate feedback processes in 19 atmospheric general circulation models, J. Geophys. Res.-Atmos., 95, 16601–16615, 1990.

Cess, R. D., Zhang, M. H., Ingram, W. J., Potter, G. L., Alekseev, V., Barker, H. W., Cohen-Solal, E., Colman, R. A., Dazlich, D. A., Del Genio, A. D., Dix, M. R., Dymnikov, V., Esch, M., Fowler, L. D., Fraser, J. R., Galin, V., Gates, W. L., Hack, J. J., Kiehl, J. T., Le Treut, H., Lo, K. K.-W., McAvaney, B. J., Meleshko, V. P., Morcrette, J.-J., Randall, D. A., Roeckner, E., Royer, J.-F., Schlesinger, M. E., Sporyshev, P. V., Timbal, B., Volodin, E. M., Taylor, K. E., Wang, W., and Wetherald, R. T.: Cloud feedback in atmospheric general circulation models: an update, J. Geophys. Res.-Atmos., 101, 12791–12794, 1996.

Colman, R.: A comparison of climate feedbacks in general circulation models, Clim. Dynam., 20, 865–873, 2003.

Danielson, J. J. and Gesch, D. B.: Global multi-resolution terrain elevation data 2010 (GMTED2010), US Geological Survey Open-File Report, 1073, 2011.

Denis, M. A., Muller, J. P., and Mannstein, H.: ATSR-2 camera models for the automated stereo photogrammetric retrieval of cloud-top heights – initial assessments, Int. J. Remote Sens., 28, 1939–1955, 2007.

Fisher, D. and Muller, J. P.: Global warping coefficients for improving ATSR co-registration, Remote Sensing Letters, 4, 151–160, 2013.

Fisher, D., Muller, J. P., and Yershov, V. N.: Automated stereo retrieval of smoke plume injection heights and retrieval of smoke plume masks from AATSR and their assessment with

AMTD
8, 5283–5327, 2015

CALIPSO and MISR, IEEE T. Geosci. Remote, 99, 1, doi:10.1109/TGRS.2013.2249073, 2014.
Garay, M. J., de Szoeke, S. P., and Moroney, C. M.: Comparison of marine stratocumulus cloud top heights in the southeastern Pacific retrieved from satellites with coincident ship-based observations, J. Geophys. Res.-Atmos., 113, D18204, doi:10.1029/2008JD009975, 2008.
Ham, S.-H., Sohn, B.-J., Yang, P., and Baum, B.: Assessment of the quality of MODIS Cloud products from radiance simulations, J. Appl. Meteorol., 48, 1591–1612, 2009.
Heidinger, A. K., Pavolonis, M. J., Holz, R. E., Baum, B. A., and Berthier, S.: Using CALIPSO to explore the sensitivity to cirrus height in the infrared observations from NPOESS/VIIRS and GOES-R/ABI, J. Geophys. Res.-Atmos., 115, D00H20, doi:10.1029/2009JD012152, 2010.
Hirschmuller, H. and Scharstein, D.: Evaluation of stereo matching costs on images with radiometric differences, IEEE T. Pattern Anal., 31, 1582–1599, 2009.
Istomina, L. G., von Hoyningen-Huene, W., Kokhanovsky, A. A., and Burrows, J. P.: The detection of cloud-free snow-covered areas using AATSR measurements, Atmos. Meas. Tech., 3, 1005–1017, doi:10.5194/amt-3-1005-2010, 2010.
Kahn, R. A., Chen, Y., Nelson, D. L., Leung, F. Y., Li, Q., Diner, D. J., and Logan, J. A.: Wildfire smoke injection heights: two perspectives from space, Geophys. Res. Lett., 35, L04809, doi:10.1029/2007GL032165, 2008.
Kiehl, J. T. and Trenberth, K. E.: Earth's annual global mean energy budget, B. Am. Meteorol. Soc., 78, 197–208, 1997.
Kiehl, J. T., Hack, J. J., and Briegleb, B. P.: The simulated Earth radiation budget of the National Center for atmospheric research community climate model CCM2 and comparisons with the Earth Radiation Budget Experiment (ERBE), J. Geophys. Res.-Atmos., 99, 20815–20827, 1994.
Llewellyn-Jones, D., Edwards, M., Mutlow, C., Birks, A., Barton, I., and Tait, H.: AATSR: Global-change and surface-temperature measurements from Envisat, Esa Bull-Eur. Space, 11–21, 2001.
Lorenz, D.: Stereoscopic imaging from polar orbit and synthetic stereo imaging, Adv. Space Res., 2, 133–142, 1982.
Marchand, R., Ackerman, T., Smyth, M., and Rossow, W. B.: A review of cloud top height and optical depth histograms from MISR, ISCCP, and MODIS, J. Geophys. Res.-Atmos., 115, D16206, doi:10.1029/2009JD013422, 2010.

AMTD
8, 5283–5327, 2015

McGill, M. J., Vaughan, M. A., Trepte, C. R., Hart, W. D., Hlavka, D. L., Winker, D. M., and Kuehn, R.: Airborne validation of spatial properties measured by the CALIPSO lidar, J. Geophys. Res.-Atmos., 112, D20201, doi:10.1029/2007JD008768, 2007.

Menzel, W. P., Smith, W. L., and Stewart, T. R.: Improved cloud motion wind vector and altitude assignment using VAS, J. Clim. Appl. Meteorol., 22, 377–384, 1983.

Menzel, W. P., Frey, R. A., Zhang, H., Wylie, D. P., Moeller, C. C., Holz, R. E., Maddux, B., Baum, B. A., Strabala, K. I., and Gumley, L. E.: MODIS global cloud-top pressure and amount estimation: algorithm description and results, J. Appl. Meteorol. Clim., 47, 1175–1198, 2008.

Moroney, C., Davies, R., and Muller, J. P.: Operational retrieval of cloud-top heights using MISR data, IEEE T. Geosci. Remote, 40, 1532–1540, 2002.

Mueller, K., Moroney, C., Jovanovic, V., Garay, M. J., Muller, J. P., Di Girolamo, L., and Davies, R.: MISR Level 2 cloud product algorithm theoretical basis, JPL Tech. Doc. D-73327, Jet Propul. Lab., Calif. Inst. of Technol., Pasadena., 2013.

Muller, J. P., Mandanayake, A., Moroney, C., Davies, R., Diner, D. J., and Paradise, S.: MISR stereoscopic image matchers: techniques and results, IEEE T. Geosci. Remote, 40, 1547–1559, 2002.

Muller, J. P., Denis, M. A., Dundas, R. D., Mitchell, K. L., Naud, C., and Mannstein, H.: Stereo cloud-top heights and cloud fraction retrieval from ATSR-2, Int. J. Remote Sens., 28, 1921–1938, 2007.

Mutlow, C. T., Murray, M. J., Bailey, P., and Birks, A.: ATSR-1/2 user guide issue 1, ESA user Guide, 2391, 1999.

Nakajima, T., Tanaka, M., and King, M. D.: Determination of the optical thickness and effective particle radius of clouds from reflected solar radiation measurements, Part I: Theory, J. Atmos. Sci., 47, 187–193, 1990.

Naud, C., Mitchell, K. L., Muller, J. P., Clothiaux, E. E., Albert, P., Preusker, R., Fischer, J., and Hogan, R. J.: Comparison between ATSR-2 stereo, MOS O2-A band and ground-based cloud top heights, Int. J. Remote Sens., 28, 1969–1987, 2007.

Poulsen, C. A., Siddans, R., Thomas, G. E., Sayer, A. M., Grainger, R. G., Campmany, E., Dean, S. M., Arnold, C., and Watts, P. D.: Cloud retrievals from satellite data using optimal estimation: evaluation and application to ATSR, Atmos. Meas. Tech., 5, 1889–1910, doi:10.5194/amt-5-1889-2012, 2012.

AMTD
8, 5283–5327, 2015

Ramanathan, V. L. R. D., Cess, R. D., Harrison, E. F., Minnis, P., Barkstrom, B. R., Ahmad, E., and Hartmann, D.: Cloud-radiative forcing and climate: results from the Earth radiation budget experiment, Science, 243, 57–63, 1989.

Rodgers, C. D.: Inverse methods for atmospheric sounding: theory and practice/series on atmospheric, Oceanic and Planetary Physics, Vol. 2, World Scientific Publishing, Singapore, 2000.

Rossow, W. B. and Garder, L. C.: Cloud detection using satellite measurements of infrared and visible radiances for ISCCP, J. Climate, 6, 2341–2369, 1993.

Rossow, W. B., Zhang, Y., and Wang, J.: A statistical model of cloud vertical structure based on reconciling cloud layer amounts inferred from satellites and radiosonde humidity profiles, J. Climate, 18, 3587–3605, 2005.

Sayer, A. M., Thomas, G. E., and Grainger, R. G.: A sea surface reflectance model for (A)ATSR, and application to aerosol retrievals, Atmos. Meas. Tech., 3, 813–838, doi:10.5194/amt-3-813-2010, 2010.

Sayer, A. M., Poulsen, C. A., Arnold, C., Campmany, E., Dean, S., Ewen, G. B. L., Grainger, R. G., Lawrence, B. N., Siddans, R., Thomas, G. E., and Watts, P. D.: Global retrieval of ATSR cloud parameters and evaluation (GRAPE): dataset assessment, Atmos. Chem. Phys., 11, 3913–3936, doi:10.5194/acp-11-3913-2011, 2011.

Seemann, S. W., Borbas, E. E., Knuteson, R. O., Stephenson, G. R., and Huang, H.-L.: Development of a global infrared land surface emissivity database for application to clear sky sounding retrievals from multi-spectral satellite radiance measurements, J. Appl. Meteorol. Clim., 47, 108–123, 2008.

Seiz, G.: Ground-and satellite-based multi-view determination of 3-D cloud geometry, Doctoral dissertation, Ph. D. thesis, Institute of Geodesy and Photogrammetry, IGP Mitteilungen, ETH Zurich, Switzerland, 2003.

Sherwood, S. C., Bony, S., and Dufresne, J. L.: Spread in model climate sensitivity traced to atmospheric convective mixing, Nature, 505, 37–42, 2014.

Shin, D. and Pollard, J. K.: Cloud height determination from satellite stereo images, in: Image Processing for Remote Sensing, IEE Colloquium on (4–1), IET, doi:doi:10.1049/ic:19960158, 1996.

Simmons, A., Uppala, S., Dee, D., and Kobayashi, S.: ERA-Interim: New ECMWF reanalysis products from 1989 onwards, ECMWF newsletter, 110, 25–35, 2007.

AMTD
8, 5283–5327, 2015

Smith, D., Mutlow, C., Delderfield, J., Watkins, B., and Mason, G.: ATSR infrared radiometric calibration and in-orbit performance, Remote Sens. Environ., 116, 4–16, 2012.
Soden, B. J. and Held, I. M.: An assessment of climate feedbacks in coupled ocean–atmosphere models, J. Climate, 19, 3354–3360, 2006.
Soden, B. J., Held, I. M., Colman, R., Shell, K. M., Kiehl, J. T., and Shields, C. A.: Quantifying climate feedbacks using radiative kernels, J. Climate, 21, 3504–3520, 2008.
Spreen, G., Kaleschke, L., and Heygster, G.: Sea ice remote sensing using AMSR-E 89 GHz channels, J. Geophys. Res.-Oceans, 113, C02S03, doi:10.1029/2005JC003384, 2008.
Stamnes, K., Tsay, S. C., Wiscombe, W., and Jayaweera, K.: Numerically stable algorithm for discrete-ordinate-method radiative transfer in multiple scattering and emitting layered media, Appl. Optics, 27, 2502–2509, 1988.
Stengel, M., Mieruch, S., Jerg, M., Karlsson, K.-G., Scheirer, R., Maddux, B., Meirink, J. F., Poulsen, C., Siddans, R., Walther, A., and Hollmann, R.: The clouds climate change initiative: assessment of state-of-the-art cloud property retrieval schemes applied to AVHRR heritage measurements, Remote Sens. Environ., 162, 363–379, doi:10.1016/j.rse.2013.10.035, 2013.
Stephens, G. L.: Cloud feedbacks in the climate system: a critical review, J. Climate, 18, 237–273, 2005.
Stocker, T. F., Qin, D., Plattner, G. K., Tignor, M., Allen, S. K., Boschung, J., Nauels, A., Xia, Y., Bex, V., and Midgley, P. M.: Climate change 2013: The physical science basis. Cambridge, UK, and New York, Cambridge University Press, 2013.
Stubenrauch, C. J., Rossow, W. B., Kinne, S., Ackerman, S., Cesana, G., Chepfer, H., Di Girolamo, L., Getzewich, B., Guignard, A., Heidinger, A., Maddux, B. C., Menzel, W. P., Minnis, P., Pearl, C., Platnick, S., Poulsen, C., Riedi, J., Sun-Mack, S., Walther, A., Winker, D., Zeng, S., and Zhao, G.: Assessment of global cloud datasets from satellites: project and database initiated by the GEWEX radiation panel, B. Am. Meteorol. Soc., 94, 1031–1049, 2013.
Vaughan, M. A., Powell, K. A., Winker, D. M., Hostetler, C. A., Kuehn, R. E., Hunt, W. H., Getzewich, B. J., Young, S. A., Liu, Z., and McGill, M. J.: Fully automated detection of cloud and aerosol layers in the CALIPSO lidar measurements, J. Atmos. Ocean. Tech., 26, 2034–2050, 2009.
Watts, P. D., Mutlow, C. T., Baran, A. J., and Zavody, A. M.: Study on cloud properties derived from Meteosat Second Generation Observations, Eumetsat Report, 2393–2403, 1998.

AMTD
8, 5283–5327, 2015

Watts, P. D., Bennartz, R., and Fell, F.: Retrieval of two-layer cloud properties from multispectral observations using optimal estimation, J. Geophys. Res.-Atmos., 116, D16203, doi:10.1029/2011JD015883, 2011.

Webb, M. J., Senior, C. A., Sexton, D. M. H., Ingram, W. J., Williams, K. D., Ringer, M. A., McAvaney, B. J., Colman, R., Soden, B. J., Gudgel, R., Knutson, T., Emori, S., Ogura, T., Tsushima, Y., Andronova, N., Li, B., Musat, I., Bony, S., and Taylor, K. E.: On the contribution of local feedback mechanisms to the range of climate sensitivity in two GCM ensembles, Clim. Dynam., 27, 17–38, 2006.

Wetherald, R. T. and Manabe, S.: Cloud feedback processes in a general circulation model, J. Atmos. Sci., 45, 1397–1416, 1988.

Wielicki, B. A., Barkstrom, B. R., Harrison, E. F., Lee III, R. B., Louis Smith, G., and Cooper, J. E.: Clouds and the Earth's radiant energy system (CERES): an earth observing system experiment, B. Am. Meteorol. Soc., 77, 853–868, 1996.

Winker, D. M., Vaughan, M. A., Omar, A., Hu, Y., Powell, K. A., Liu, Z., Hunt, W. H., and Young, S. A.: Overview of the CALIPSO mission and CALIOP data processing algorithms, J. Atmos. Ocean. Tech., 26, 2310–2323, 2009.

Zabih, R. and Woodfill, J.: Non-parametric local transforms for computing visual correspondence, in: Computer Vision – ECCV'94, Springer Berlin, Heidelberg, 151–158, 1994.

Zelinka, M. D., Klein, S. A., Taylor, K. E., Andrews, T., Webb, M. J., Gregory, J. M., and Forster, P. M.: Contributions of different cloud types to feedbacks and rapid adjustments in CMIP5*, J. Climate, 26, 5007–5027, 2013.

AMTD
8, 5283–5327, 2015

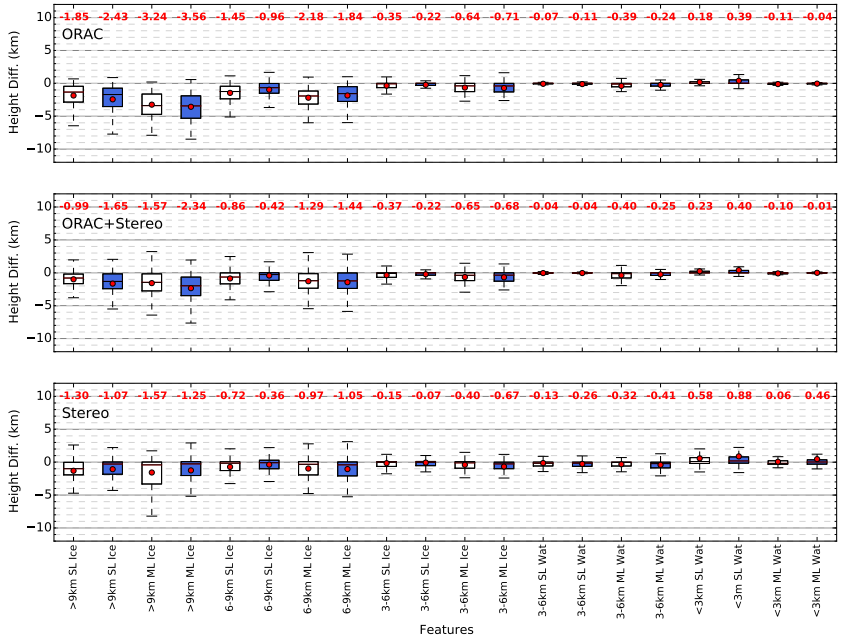

Figure 1. The top box-and-whisker plot provides a statistical summary of the comparison of the ORAC CTH retrieval vs. collocated CALIOP observations derived through the process discussed in Sect. 5.1. The middle plot provides a statistical summary of the ORAC+Stereo CTH comparison against CALIOP and the bottom plot the summary of the stereo CTH against CALIOP. The box-and-whisker plots follow standard conventions. The whiskers represent 1.5 times the IQR of the upper and lower quartiles. The red circles represent the mean. White boxes are for collocated observations over ice; blue boxes for collocated observations over water. The features which define the comparisons are presented along the *x* axis, where: *ML* is multi-layer cloud and *SL* is single layer cloud; *ice* indicates ice-cloud and *wat* indicates water cloud; the elevation range of clouds included in each box analysis is determined by the elevation of the uppermost CALIOP CTL. In all cases the order of operation employed is subtraction of the CALIOP CTL from the AATSR derived CTH.

AMTD
8, 5283–5327, 2015

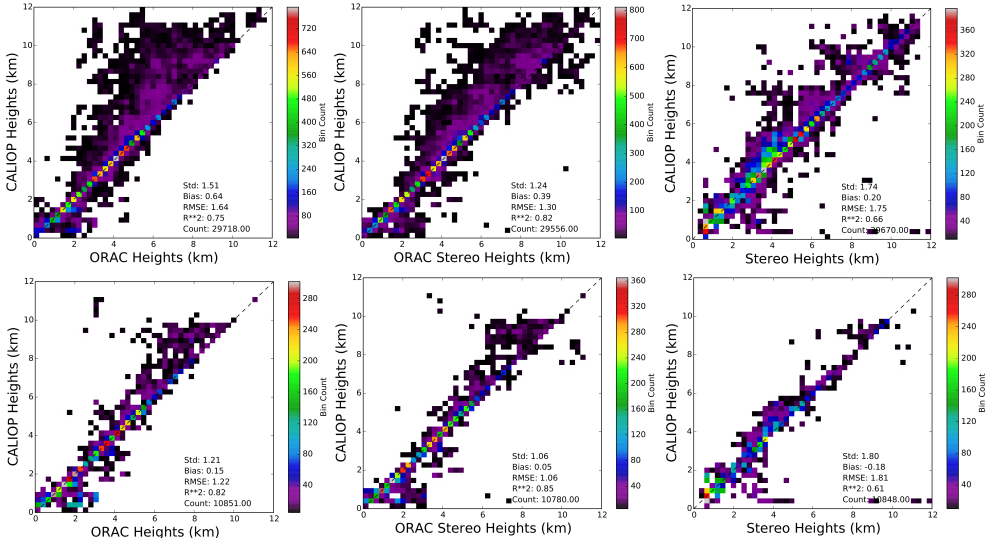

Figure 2. These plots contain the histogram analyses of CALIOP vs. ORAC, ORAC+Stereo and stereo. The upper row of histograms plots all available inter-comparison data. The bottom row of histograms plots the inter-comparison data following a screening process, where only those collocations with single-layer clouds (as determined by CALIOP) and surface ice concentrations of zero (as determined by AMSR-E) are considered. To be displayed the bin must contain more than 10 samples.

AMTD
8, 5283–5327, 2015

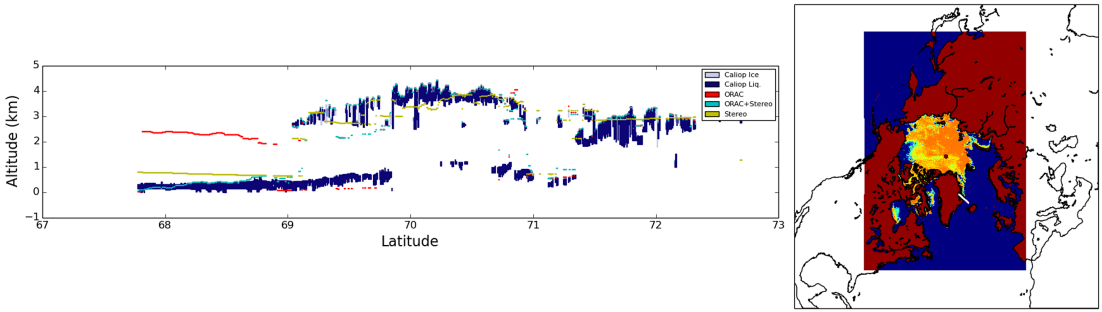

Figure 3. This profile plot show the 1 km CALIOP cloud profile for orbit with the time stamp 2008-07-05T13-02-15ZD. Over plot are the collocated CTH data from ORAC, ORAC+Stereo, and census stereo. The key in the plot indicates the relationship between colour and feature type. The white line off the east coast of Greenland indicates the location of the profile shown in the profile plot (the data is obtained from the AMSR-E sea-ice product for the day defined by the CALIOP data).

AMTD
8, 5283–5327, 2015

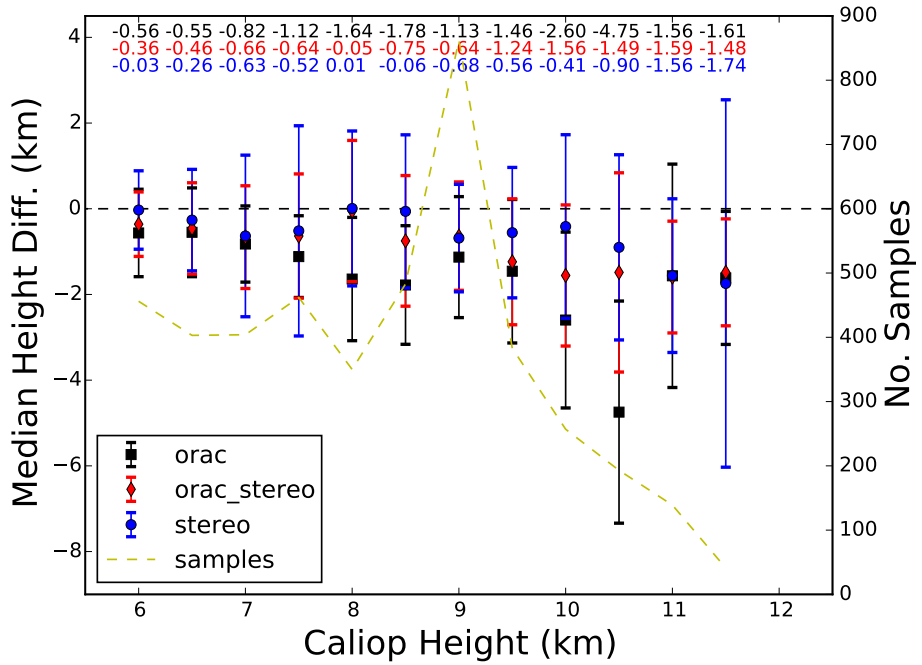

Figure 4. Error bar plot plotting the median height differences for single-layer ice clouds at or above 6 km (as determined by CALIOP) for the three algorithms applied to AATSR and the elevation of the CALIOP CTL, as a function of the elevation of the CALIOP CTL at 500 m intervals (in this instance the median is derived from all collocated data contained within set given by the CALIOP CTL elevation indicated on the x axis and all CALIOP CTL samples which are located within the following 500 m, e.g. 6 km $\leq$ CTL $<$ 6.5 km). The three statistics above each error bar are the median differences. The error-bar whiskers represent 1 SD.

AMTD
8, 5283–5327, 2015

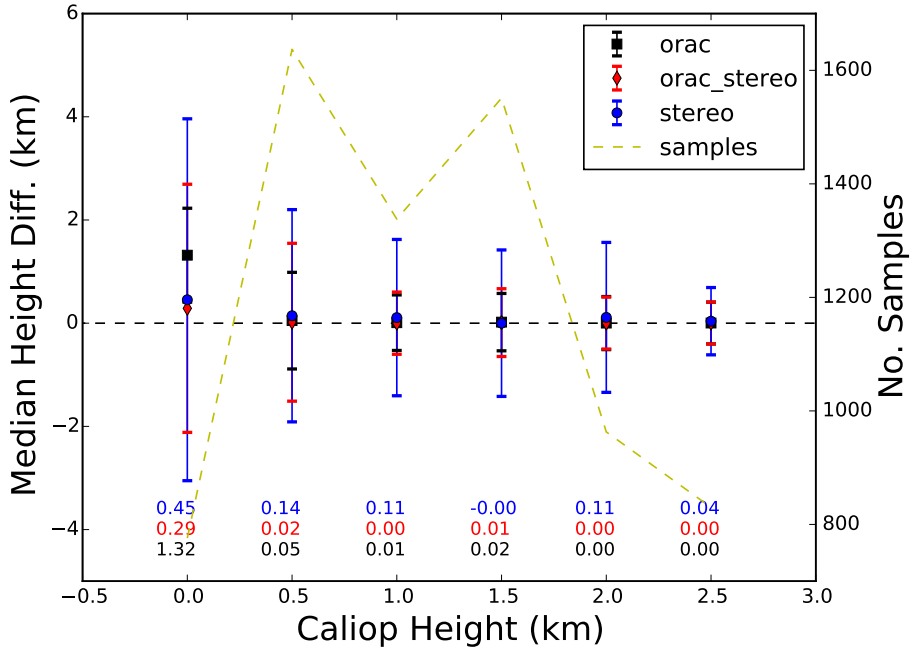

Figure 5. Error bar plot plotting the median height differences for single-layer water clouds below 3 km (as determined by CALIOP) for the three algorithms applied to AATSR and the elevation of the CALIOP CTL, as a function of the elevation of the CALIOP CTL at 500 m intervals (in this instance the median is derived from all collocated data contained within set given by the CALIOP CTL elevation indicated on the x axis and all CALIOP CTL samples which are located within the following 500 m, e.g. 0 km $\leq$ CTL $<$ 0.5 km). The three statistics below each error bar are the median differences. The error-bar whiskers represent 1 SD.

AMTD
8, 5283–5327, 2015

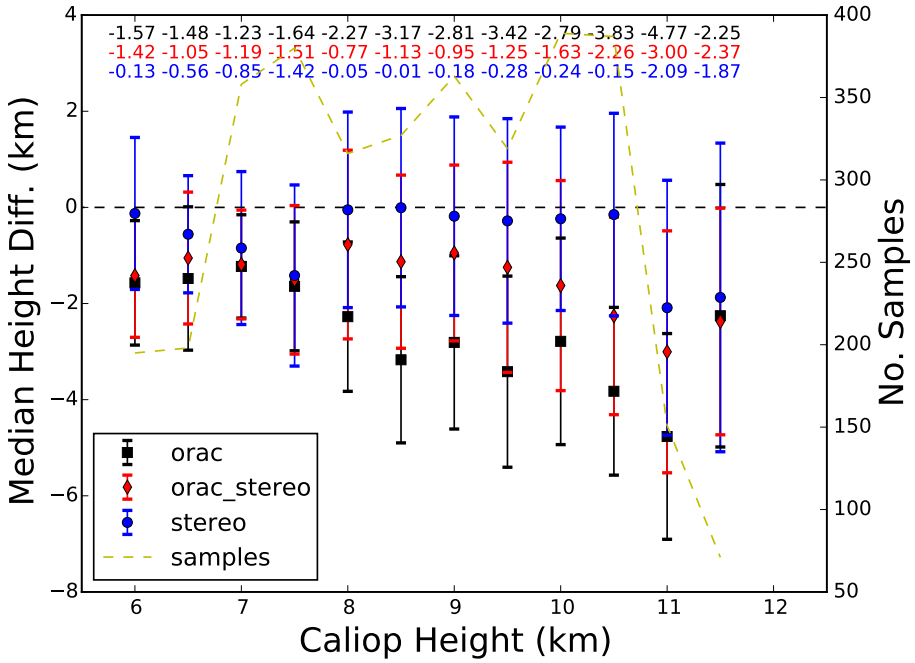

Figure 6. Error bar plot plotting the median height differences for multi-layer ice clouds at or above 6 km (as determined by the uppermost CALIOP CTL elevation) for the three algorithms applied to AATSR and the elevation of the uppermost CALIOP CTL, as a function of the elevation of the uppermost CALIOP CTL at 500 m intervals (in this instance the median is derived from all collocated data contained within set given by the uppermost CALIOP CTL elevation indicated on the x axis and all uppermost CALIOP CTL samples which are located within the following 500 m, e.g. 6 km $\leq$ CTL $<$ 6.5 km). The three statistics above each error bar are the median differences. The error-bar whiskers represent 1 SD.

AMTD
8, 5283–5327, 2015

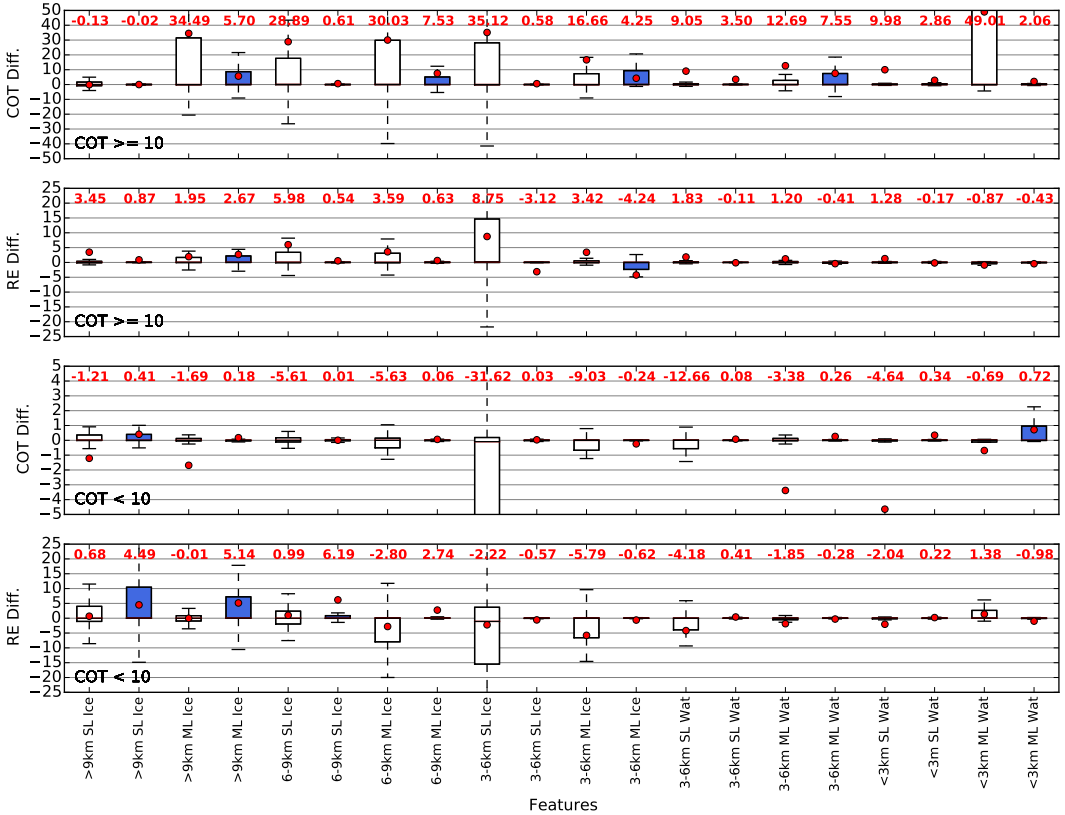

AMTD
8, 5283–5327, 2015

Synergistic cloud property retrieval

D. Fisher et al.

Figure 7. The top box-and-whisker plot provides a statistical summary of the differences between the ORAC and ORAC+Stereo cloud optical depth retrievals for the dataset derived in the CTH evaluation for cloud optical depth of greater than 10. The second plot provides a statistical summary of the differences between the ORAC and ORAC+Stereo effective radius retrievals, also for cloud optical depths of greater than 10. The third and fourth plots plot the statistical summary of the differences for COD and RE for cloud with optical depth of less than 10 respectively. The box-and-whisker plots follow standard conventions. The whiskers represent 1.5 times the IQR of the upper and lower quartiles. Outliers are not plotted here as they are substantial and significant, and dominate the plots. The red circles represent the mean, which is also given by the red statistic at the top of each box-and-whisker plot. White boxes are for collocated observations over ice; blue boxes for collocated observations over water. For some of the boxes, it is difficult to determine whether it is snow of ice, however they run in an alternating fashion, starting from ice. The features which define the comparisons are presented along the *x* axis, where: *ML* is multi-layer cloud and *SL* is single layer cloud; *ice* indicates ice-cloud and *wat* indicates water cloud; the elevation range of clouds included in each box analysis is determined by the elevation of the uppermost CALIOP CTL. The order of operation employed in this figure is the subtraction of the ORAC+Stereo microphyiscal parameters from the ORAC microphysical parameters for each assessment.

AMTD
8, 5283–5327, 2015

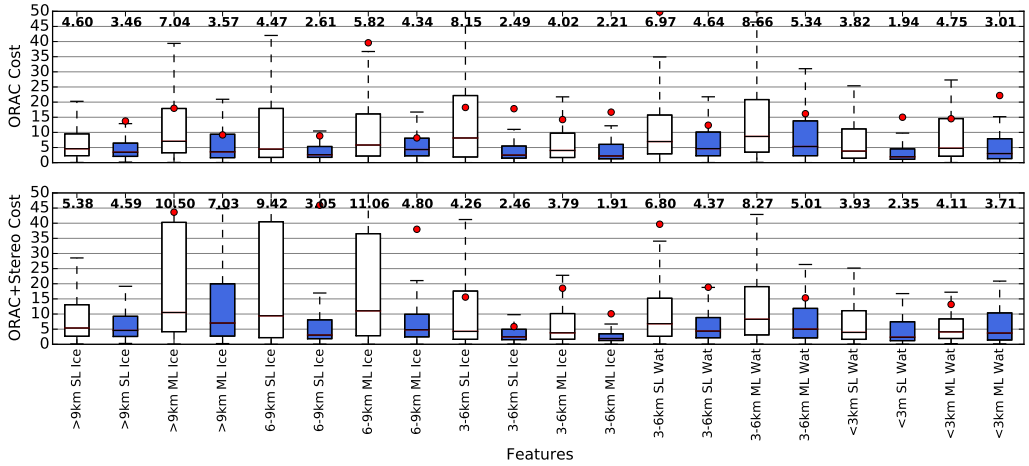

Figure 8. The top box-and-whisker plot provides a statistical summary of the ORAC cost for the described cloud features. The second plot provides a statistical summary of the ORAC+Stereo cost for the same cloud features. The box-and-whisker plots follow standard conventions. The whiskers represent 1.5 times the IQR of the upper and lower quartiles. Outliers are not plotted here as they are substantial and significant, and dominate the plots. The red circles represent the mean. The black statistic which at the top of each box-and-whisker plot is the median cost. White boxes are for collocated observations over ice; blue boxes for collocated observations over water. For some of the boxes, it is difficult to determine whether it is snow of ice, however they run in an alternating fashion, starting from ice. The features which define the comparisons are presented along the *x* axis, where: *ML* is multi-layer cloud and *SL* is single layer cloud; *ice* indicates ice-cloud and *wat* indicates water cloud; the elevation range of clouds included in each box analysis is determined by the elevation of the uppermost CALIOP CTL.

AMTD
8, 5283–5327, 2015

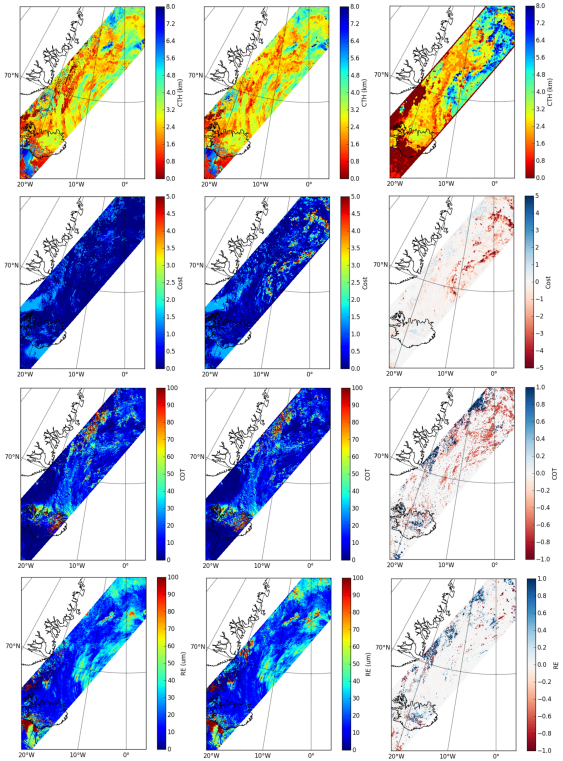

Figure 9. The top row of maps show CTH as retrieved by ORAC, ORAC+Stereo and census stereo from left to right. The second row of maps shows the cost associated with each retrieved pixel, with the left plots the costs for ORAC, the central map plots the costs for ORAC+Stereo, and the right map plots the difference between the costs. The third row shows the COT maps, with the same arrangement as the second row. The fourth row shows the RE maps with the same arrangement as the above two rows. All the data employed comes from the processed AATSR orbit collocated with the CALIOP profile presented in Fig. 3.

AMTD
8, 5283–5327, 2015